Mining Science, vol. 29, 2022, 121–144

www.miningscience.pwr.edu.pl

Mining Science

(Previously Prace Naukowe Instytutu Gornictwa Politechniki Wroclawskiej, ISSN 0370-0798)

ISSN 2300-9586 (print)
ISSN 2353-5423 (online)

Received November 11, 2021; Reviewed; Accepted September 20, 2022

INVESTIGATION ON ROCK CUTTING CHARACTERISTICS OF SPHERICAL-TOOTH HOB

Xuhui Zhang[1], Zhaomin Long[1, 2], Yashi Liao[1]*, Jinjing Long[1], Jifu Liu[1]

[1.] College of Engineering and Design, Hunan Normal University, Changsha, 410081, China;

[2.] College of Mechanical and Electrical Engineering, Central South University, Changsha Hunan 410083, China

Abstract: To study the rock cutting characteristics of spherical-tooth hob, the rock cutting process induced by the spherical-tooth hob is analyzed based on the finite element simulation and the rock cutting experiments. Then the rock breaking states, rock cutting forces and rock cutting efficiency caused by the spherical-tooth hob under different penetrations are obtained. The results show that a cutting groove and a series of pits in the cutting groove will be produced when the penetration exceeds 9 mm. At such penetration, the spherical teeth and the cutter ring can cooperate to cut rock. The cutting forces curves show obvious fluctuation and the peak va*Corresponding author: e-mail address: liaoyashi6666@hunnu.edu.cn
lues of cutting forces correspond to the moment when a spherical tooth intrudes into the rock sample totally. The cutting forces increase with the growth of the penetration and the increase speed turns fast when the penetration exceeds 9 mm. With the increase of penetration, the specific energy consumption of the spherical-tooth hob first decreases and then increases. It exists an optimal penetration of 12 mm to achieve the highest rock cutting efficiency.

Key words: *Spherical-tooth hob; Penetration; Rock cutting force; Specific energy consumption*

* Corresponding author: e-mail address: liaoyashi6666@hunnu.edu.cn

doi: 10.37190/msc222908

1. INTRODUCTION

Tunnel boring machine (TBM) is a typical kind of large-scale construction machine used for excavating tunnel, in which the hob is the main tool for TBM to cut rock (Lin, et al., 2020; Xia, et al., 2021; Zhang, et al., 2021a). Therefore, the rock cutting performance of the TBM hob directly affects the overall excavation performance of the TBM. In order to improve the rock cutting performance of TBM hobs, a large number of researches have been carried out on the rock cutting law of the TBM hobs. At present, the rock cutting experiment and rock cutting simulation by TBM hob are the main research methods.

In terms of rock cutting experiment by TBM hob, Gertsch et al. (2007) presented the variation of rock cutting forces and rock breaking specific energy of TBM hob under different parameters based on linear cutting test-bed. Cho et al. (2013) carried out linear cutting experiments with TBM hob under different parameters to obtain the optimal rock cutting parameters under granite conditions. Xia et al. (2012) investigated the change regulation of rock cutting forces of the TBM hob under different installation radius by using rotary rock cutting test-bed. Tumac and Balci (2015) studied the rock cutting characteristics of the TBM hob based on the linear cutting tests. Entacher et al. (2015) displayed the rock breaking patterns and crack propagation features beneath the TBM hob. Geng et al. (2016a) analyzed the rock cutting forces of edge TBM hob based on the rotary test-bed. Pan et al. (2019a, 2018, 2019b) performed linear cutting tests to study the rock cutting forces of the TBM hob. Lin et al. (2019, 2018) provided the indentation force and acoustic emission characteristics of the TBM hob based on the indentation experiments. Liu et al. (2018a) conducted the rock indentation tests to study the effects of surface and internal crack propagation on rock breakages by TBM hob. Cardu et al. (2021) discussed the optimal cutting condition and the size distribution of the debris combined with the cutting tests of the TBM hob. The rock cutting experiment of TBM hob is an effective method to investigate the rock breaking characteristics and its result can be applied in TBM engineering site directly, which has a good reference value for the optimal design and layout of TBM hob on rock cutting.

In terms of rock cutting simulation by TBM hob, Cho et al. (2010) used the AUTODYN-3D to simulate the rock cutting process of the TBM and verified the reliability of the simulation model by test results. Xia et al. (2017) employed the AUTODYN-3D to study the influence of the free surface on the rock fragment. Zhai et al. (2016) proposed a meshfree numerical method to investigate the rock fragment by

TBM hobs. Haeri et al. (2016) simulated the crack propagation and cracks coalescence induced by TBM hobs. Zare et al. (2017) optimized the rock cutting spacing in jointed rock with UDEC. Liu et al. (2019a) and Zhang et al. (2021b) reported the indentation characteristics of the TBM hob with different blade types based on the PFC software. Geng et al. (2017) and Xiao et al. (2017) explored the rock breaking process by TBM hob with ABAQUS. Xue et al. (2021) simulated the rock fragment by the TBM hob considering the joint effect with MatDEM. Rock cutting simulation by TBM is also a promising way to study the rock cutting characteristics and its results have been widely proved by the rock cutting experiments of the TBM hob. Hence, it is feasible and reliable to analyze the rock cutting characteristics of the TBM hob by simulation method.

At present, the rolling cutting tools used for rock cutting in TBM mainly include constant-section hob and spherical-tooth hob, as shown in Fig. 1. The spherical-tooth hob has a series of spherical teeth on the cutter ring compared with the constant-section hob. During the rock cutting process by the spherical-tooth hob, the spherical-tooth hob can crush the rock face in advance for the cutter ring and it has a small contact area between the hob and the rock. Therefore, the spherical-tooth hob has great potential in improving the rock cutting performance of the TBM. However, the researches on rock cutting characteristics TBM hobs are mainly concentrated in constant-section hobs based above literature analysis. There are also a few researches on rock cutting characteristics of spherical-tooth cutter. For instance, Tan et al. (2010) and Deng et al. (2020) simulated the crack propagation induced by the spherical tooth in two-dimensional condition. Hu et al. (2019) built a three-dimensional model with LS-DYNA to analyze the rock cutting process caused by a spherical-tooth hob with multiple rows of teeth. Zou et al. (2022) explored the boreability and crushing efficiency caused by the indentation of the inserted tooth cutter. Wu et al. (2018) conducted rotary cutting test of a spherical-tooth hob with multiple rows of teeth to study the rock breaking process. These researches can greatly promote the comprehension on the rock cutting characteristics of the spherical-tooth hob. However, the rock breaking mechanism, rock cutting characteristics about the spherical-tooth hob in TBM field is still unclear, especially the influence of the penetration on rock cutting force and energy consumption of the spherical-tooth hob is not revealed.

Consequently, it is necessary to investigate the rock cutting characteristics of the spherical-tooth hob deeply and enrich the understanding about influence of the hob penetration on rock cutting force and cutting energy. In this paper, the three-dimensional simulation model of rock cutting by spherical-tooth hob is established through the finite

element method of ABAQUS firstly. Then, the rock cutting process induced by the spherical-tooth hob is studied, the rock cutting force and rock cutting efficiency of the spherical-tooth hob under different penetrations are also analyzed in this paper. Furthermore, the rock cutting experiments induced by the spherical-tooth hob are conducted to support and enrich the simulated results. The research results can provide reference for improving the rock cutting performance of spherical-tooth hob and the tunneling efficiency of the TBM.

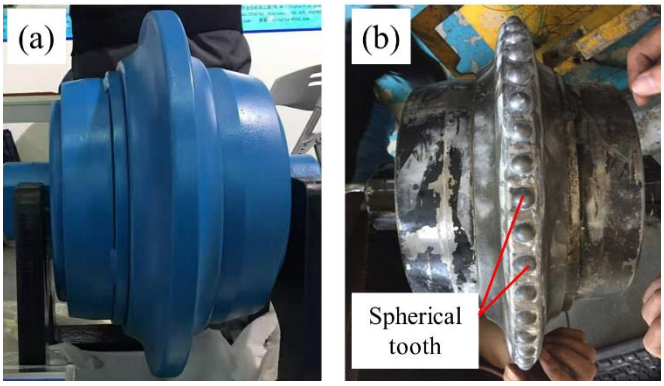

Fig. 1. Two kinds of TBM hob: (a) constant-section hob; (b) spherical-tooth hob

2. ROCK CUTTING MODEL OF SPHERICAL-TOOTH HOB

2.1. GEOMETRIC PARAMETERS OF SPHERICAL-TOOTH HOB

In this paper, the spherical-tooth hob with a diameter of about 17 inches is used in the cutting simulation. The cutter ring and spherical-tooth structure of the hob are shown in Fig. 2. 36 spherical teeth with a radius of 9 mm are evenly distributed at the circumference of the cutter ring. The spherical tooth spacing (S) and the blade width (T) of the spherical-tooth hob are 40 mm and 20 mm, respectively. The spherical-tooth hob in the simulation is set as a rigid body since only the rock cutting force and rock cutting energy are considered instead of the wear and deformation of the spherical-tooth hob.

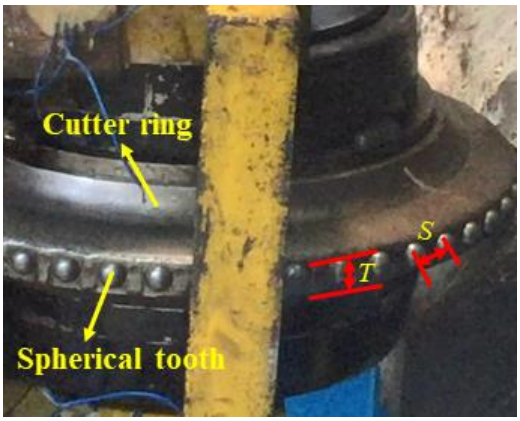

Fig. 2. Spherical-tooth hob used in rock cutting model

2.2. ROCK CONSTITUTIVE MODEL

The simulated rock sample in this paper is rust stone, with compressive strength of 76.8 MPa, elastic modulus of 30.3 GPa and density of 2.44g/cm^3. The deformation of the rock sample in elastic stage can be defined by elastic modulus and Poisson's ratio. The deformation of the rock sample in plastic stage is described by the Drucker-Prager constitutive mode in ABAQUS (Liu, et al. 2019b). The yield function of the Drucker-Prager constitutive plastic model is as follows.

$$q - ptan\beta - d = 0 \tag{1}$$

$$q = \sigma_1 - \sigma_3 \tag{2}$$

$$p = \frac{1}{3}(2\sigma_1 + \sigma_3) \tag{3}$$

Where q is the Mises equivalent stress, p is the mean stress, β is the friction angle of the rock material with a value of 50°, d is the cohesion of the rock material with a value of about 46.3 MPa, σ_1 is the first principal stress, σ_3 is the third principal stress.

The damage and failure process of rock element is shown in Fig. 3 (Liu, et al. 2018b), which can be controlled by the E calculated by Eq. 4. In this equation, $\bar{E}$ is the initial elastic modulus, D is the damage factor. At point C, the rock begins to damage, as shown in Fig. 3. When the fracture damage reaches point D, the damage factor D = 1, then E = 0, and the rock element is deleted from the grids. The compressive hardening is adopted as the yield criterion of the rock sample, and the fracture strain is 0.003.

$$E = \bar{E}(1 - D) \tag{4}$$

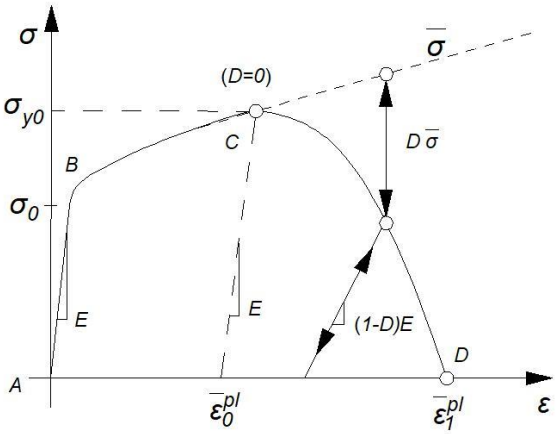

Fig. 3. Failure process curve of the rock element

2.3. FIELD OUTPUT AND BOUNDARY CONDITION

The field variable outputs include the damage value, spatial displacement, spatial velocity, etc. The history outputs consist of rock cutting forces, as shown in Fig. 4. Only the vertical and rolling forces are investigated in this study since the lateral force is around 0 for the linear cutting simulation. The contact relationship is described by customized general contact method in ABAQUS, and the friction coefficient between the hob and the rock is set to 0.3.

The revolution point RP1 and the reference point RP of the hob are established and connected with a hinge connector which is used to simulate the spherical-tooth hob axis, as shown in Fig. 5. Therefore, the rock cutting movement of the spherical-tooth hob is controlled by the revolution point RP1. A local coordinate system is established on point RP1. The X axis of the local coordinate system coincides with the hinge connector. The freedoms of the point RP1 rotating around the X axis and moving in Z direction (rolling direction shown in Fig. 4) are free, while other freedoms of the point RP1 are constrained. Thus, the spherical-tooth hob can rotate around its own cutter shaft under the action of friction and move along the Z direction by the applied cutting speed. The bottom of the rock sample is limited to realize the fixation of the rock. The size of the rock sample is 200mm×200mm×50 mm.

The C3D10M mesh element is used for spherical-tooth hob, which belongs to second-

order element. This kind of mesh element has good adaptability to complex areas and good contact accuracy. The rock is divided by C3D8R mesh element. Because the rock is a brittle material, the hourglass control is adopted to avoid the distortion of the mesh element in the cutting process. To improve the simulation efficiency, mesh refinement is used in the contact area of rock where the minimum element length is 3mm, as shown in Fig. 5. In addition, to facilitate the statistics of rock breaking volume, the rock mesh element deletion function is turned on.

The computing time used by cutting simulation increases exponentially with the increase of the cutting speed of the hob. Some researchers (Geng et al. 2016b; Jiang et al. 2021) have reported and confirmed that the cutting speed varied within 10 m/s has little effect on rock cutting force and rock cutting energy consumption in finite element simulation. Therefore, the cutting speed of the spherical-tooth hob in the rolling direction is set to 300 mm/s in cutting simulations considering the simulation efficiency and accuracy. The cutting time is set to 1.0 s during cutting simulation process. Furthermore, five kinds of penetrations with values of 3, 6, 9, 12 and 15mm are selected in these cutting simulations.

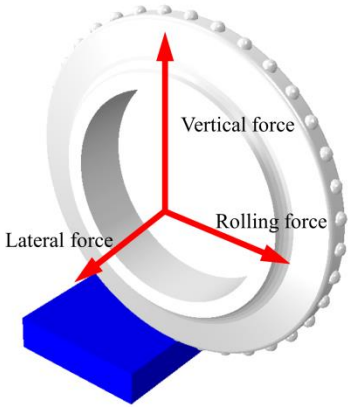

Fig. 4. Schematic diagram of cutting force of hob

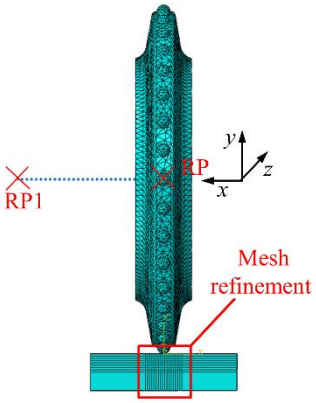

Fig. 5. Relationship of point RP1 and the point RP

3. ANALYSIS OF ROCK CUTTING RESULTS BY SPHERICAL-TOOTH HOB

3.1. ROCK BREAKING PROCESS INDUCED BY SPHERICAL-TOOTH HOB

The rock breaking process induced by the spherical-tooth hob at the penetration of 6 mm is illustrated in Fig. 6. Fig 6 (a) shows the second pit is just formed, and the cutting forces reaches the peak value, as depicted by the circle a in Fig. 7. With the continuous rolling of the spherical-tooth hob, the rock element beneath the spherical tooth will be failed and then be deleted (Fig 6 (b)), leading to a decline in vertical force, as displayed by the circle b in Fig. 7. When the cutting time approaches 0.35 s, the third spherical tooth begins to touch the rock sample (Fig 6 (c)), and the cutting forces will also raise rapidly (Fig. 7). Subsequently, the third pit will follow the formation of the second pit, accompanied by a decline of the cutting forces, as shown in Fig 6 (d) and Fig. 7. It can be concluded that the peak value of the vertical and rolling forces correspond to the moment when a spherical tooth intrudes into the rock sample totally.

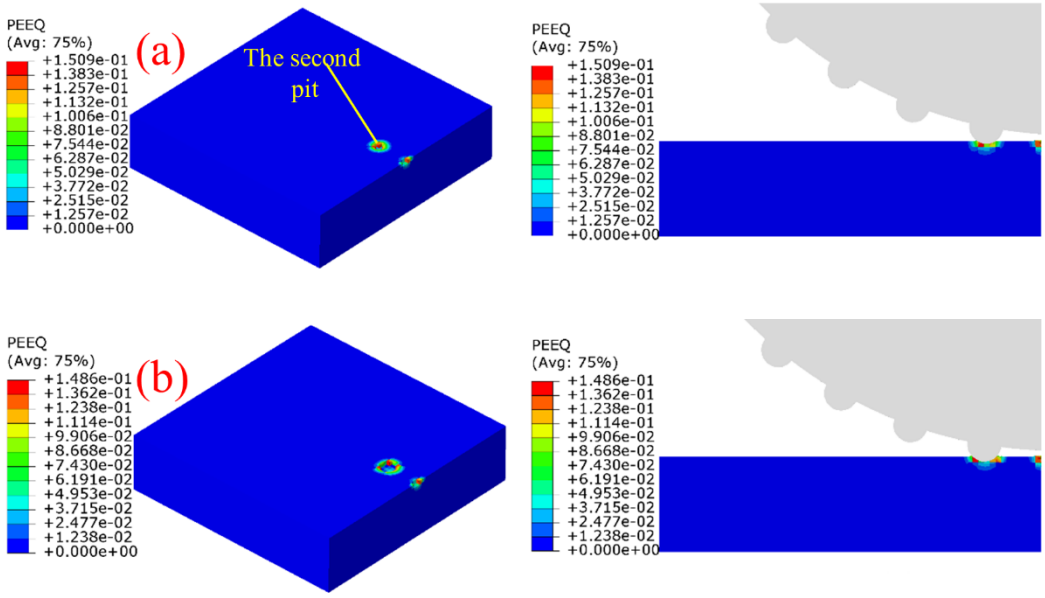

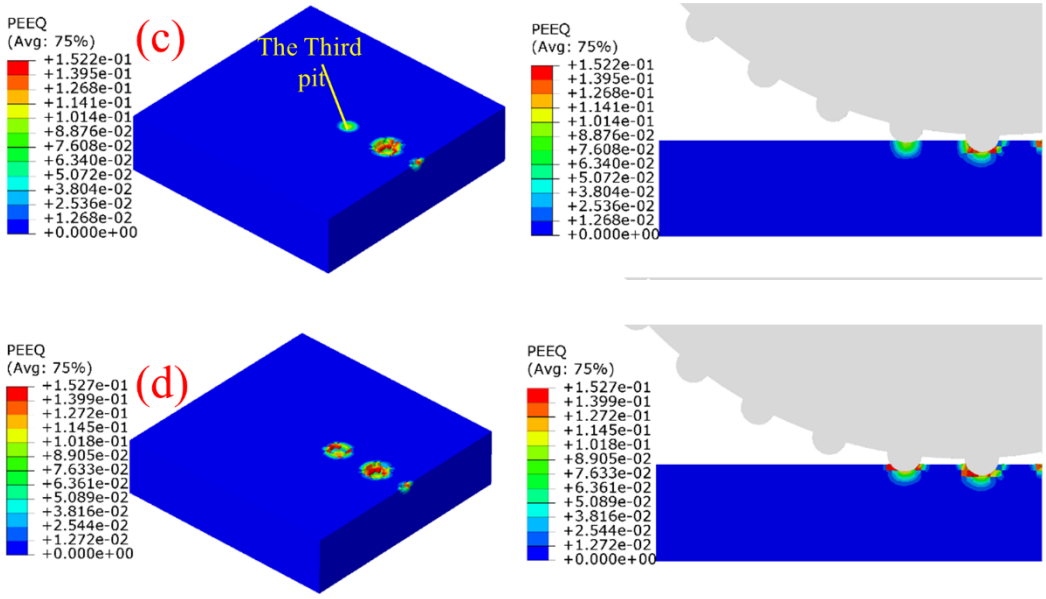

Fig. 6. Rock breaking process at the penetration of 6mm: (a) t=0.21s; (b) t=0.23s; (c) t=0.35s; (d) t=0.40s

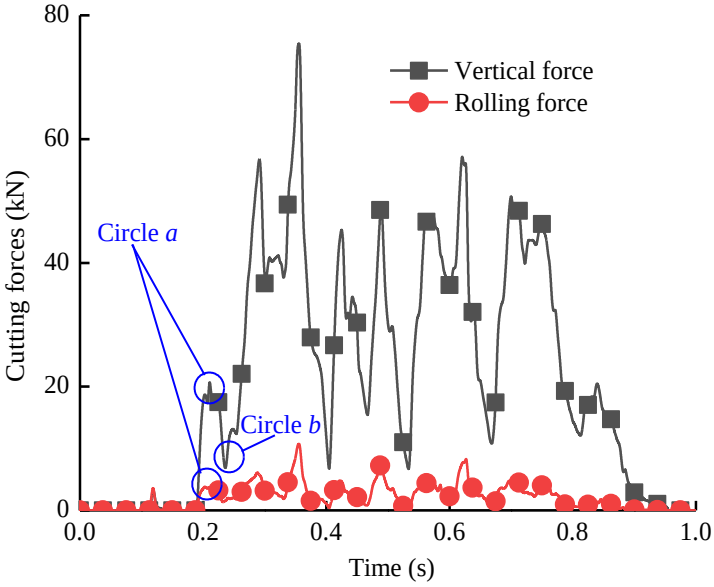

Fig. 7. Rock cutting forces at the penetration of 6 mm

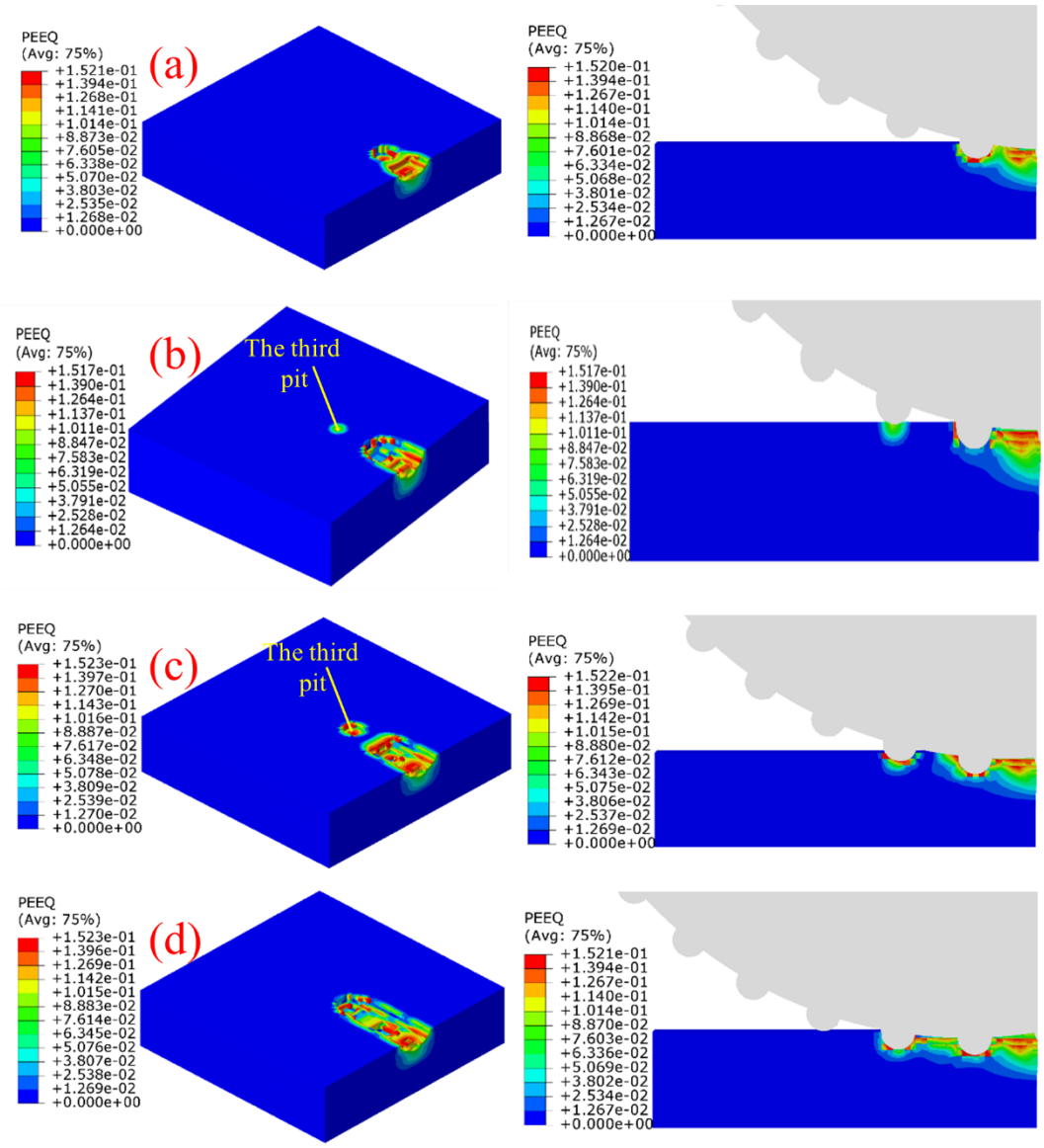

Fig. 8. Rock breaking state at the penetration of 12mm: (a) t=0.22s; (b) t=0.27s; (c) t=0.31s; (d) t=0.38s

Fig. 8 presents the rock breaking process at the penetration of 12 mm. At this penetration, the cutter ring could cut the rock sample, the cutter ring and the spherical teeth seem to work together to cut rock, as shown in Fig. 8 (a). At the time of 0.27s (Fig. 8 (b)), the third pit is in the initial stage of its formation. With the continuous rolling of

the spherical-tooth hob, the spherical tooth completely presses into the rock (Fig. 8 (c)), causing a peak value of the cutting forces, as displayed by the circle c in Fig. 9. On the basis of pre crushing of the spherical tooth, then the cutter ring contact and cut the rock sample. Therefore, the generated pits can relieve the loading condition of the cutter ring. When the rock cutting process is finished, a cutting groove and some pits in the cutting groove are left on the rock sample due to the comprehensive cutting effect of spherical-tooth and cutter ring, as presented in Fig. 8 (d). These rock breaking phenomena will be further investigated in next sections.

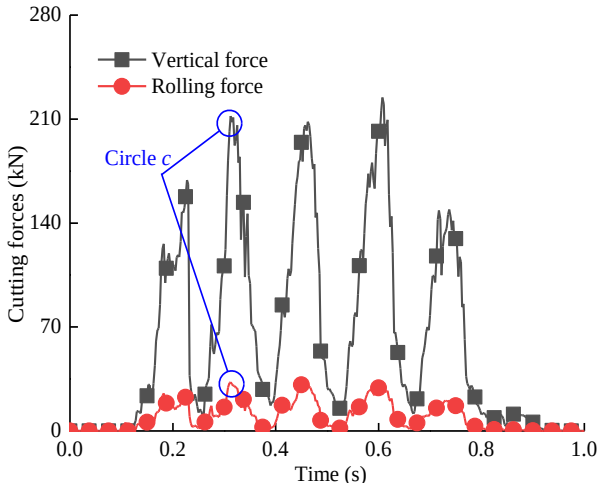

Fig. 9. Rock cutting forces at the penetration of 12 mm

3.2. INFLUENCE OF PENETRATION ON ROCK BREAKING STATE

The rock breaking states under different penetrations are shown in Fig. 10. The spherical-tooth hob could lead to greater damage to the rock with the increase of the penetration. When the penetration is less than or equal to 9 mm, some obvious pits caused by the spherical teeth can be found on the rock sample, as shown in Fig. 10 (a), (b) and (c). In these pits, the maximum contact stress is at the bottom of the pit, as described with the red stress area. It can also be observed that the rock between the adjacent pits could not be detached from the rock sample. It implies that the spherical tooth spacing is too large to produce synergistic rock breaking effect between spherical teeth. When the penetration is greater than 9mm, both the spherical teeth and cutter ring can cut the rock sample since the value of the penetration is larger than that of the spherical-tooth height,

as shown in Fig. 10 (d) and (e). Moreover, a cutting groove and some pits are generated, indicating that the spherical teeth and cutter ring can cooperate to cut rock sample at a large penetration. This rock cutting process can be summarized as that the spherical teeth first press out the pits, causing a lot of damage to the rock in the pit area. Then, the cutter ring cuts the rock along the path of the spherical teeth, which can relieve the rock cutting forces of the spherical-tooth hob, which is coincided with the analysis results in Section 3.1.

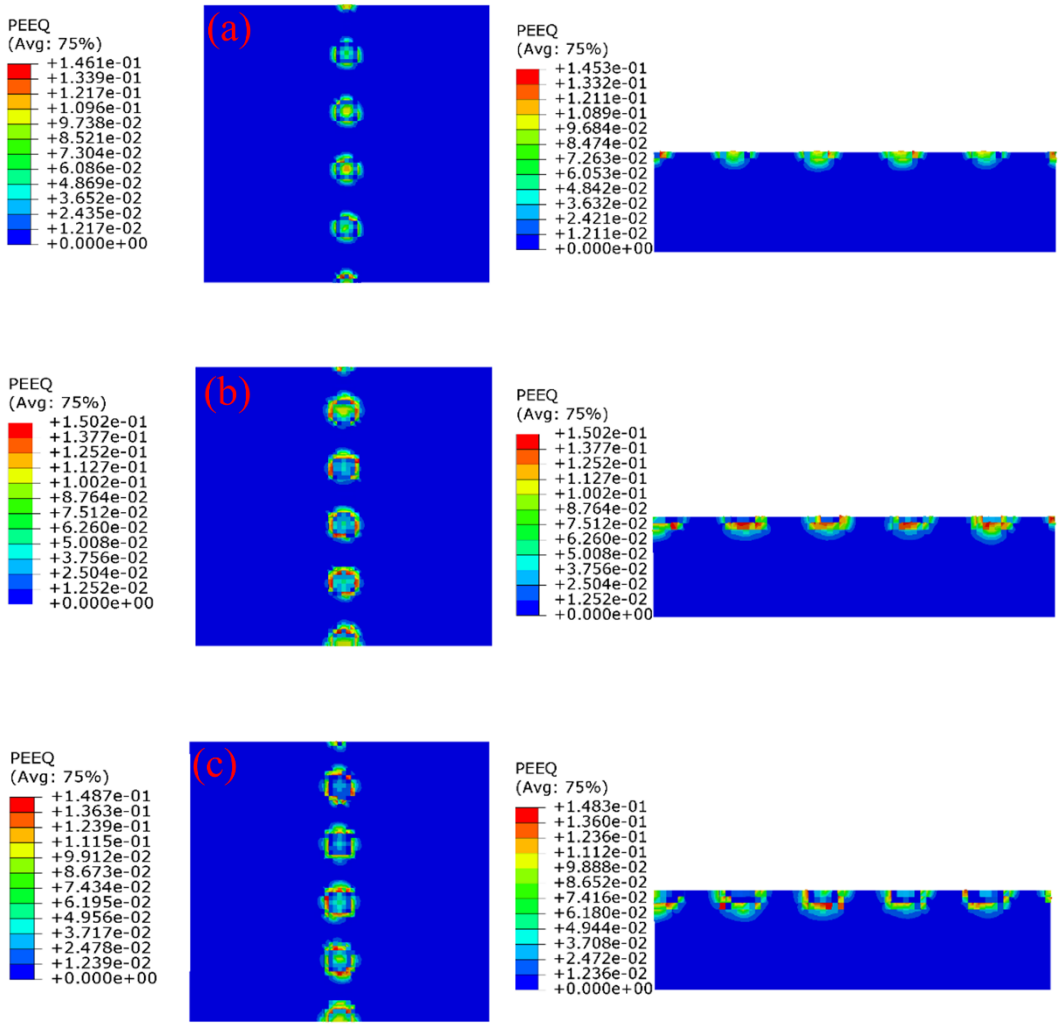

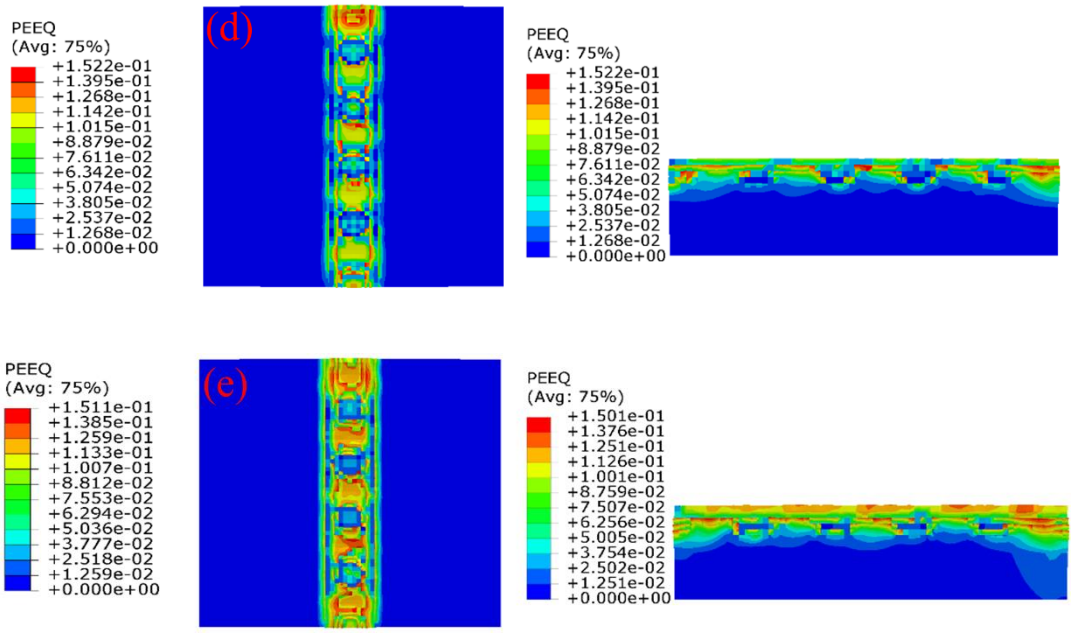

Fig. 10. Rock breaking states under different penetrations: (a) penetration =3mm; (b) penetration =6mm; (c) penetration =9mm; (d) penetration =12mm; (e) penetration =15mm

3.3. INFLUENCE OF PENETRATION ON ROCK CUTTING FORCE

The vertical and rolling forces curves with time under different penetrations are depicted in Fig. 11 and Fig. 12, respectively. Both the vertical and rolling forces fluctuate obviously with the development of the rock cutting time. The minimum value of vertical and rolling forces will not arrives at zero since there will always be a spherical tooth in contact with the rock sample during the cutting process, which will not cause all unloading, as described in Fig. 6 and Fig. 8. It should be noted that the fluctuation amplitude of these two kinds of forces shows an upward trend with the growth of the penetration. For instance, the fluctuation amplitude of vertical force at penetration of 3 mm is approximate 40.0 kN, while the fluctuation amplitude of vertical force at penetration of 12 mm is about 180.0 kN. It is not hard concluded that the vertical force is much larger than the rolling force by comparing Fig. 11 and Fig. 12, reflecting that the rock breaking process of the spherical-tooth hob is mainly driven by vertical force.

The average vertical force and rolling force under different penetrations are presented in Fig. 13. With the growth of the penetration, both the average vertical force and the

average rolling force of the spherical-tooth hob increase exponentially. The increase speed of the average vertical and rolling forces turns faster when the penetration exceeds 9 mm. It can be explained that the cutter ring could touch and cut the rock sample at these penetrations, producing a larger contact surface between the spherical-tooth hob and rock sample, and causing a larger increase amplitude in average vertical and rolling forces. For instance, when the penetration is less than 9 mm, the vertical and rolling forces increase by about 11.1 kN and 1.3 kN for every 3 mm growth in penetration, respectively. While the penetration exceeds 9 mm, the vertical and rolling forces increases by about 35.5 kN and 7.1 kN for every 3 mm growth in penetration, respectively. It also can be observed that the growth amplitude of the vertical force is much larger than that of the rolling force, and the difference between vertical force and rolling force presents an upward trend with the growth of the penetration. For example, when the penetration is 3 mm, the difference between vertical force and rolling force is about 8.0 kN. While the penetration reaches 12 mm, the difference between vertical force and rolling force is about 51.5 kN.

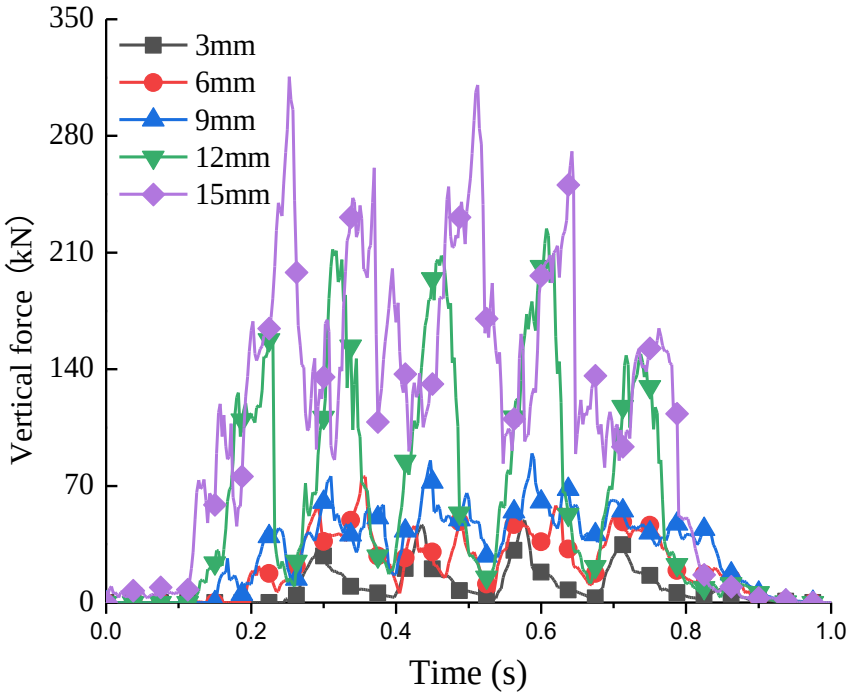

Fig. 11. Vertical force under different penetrations

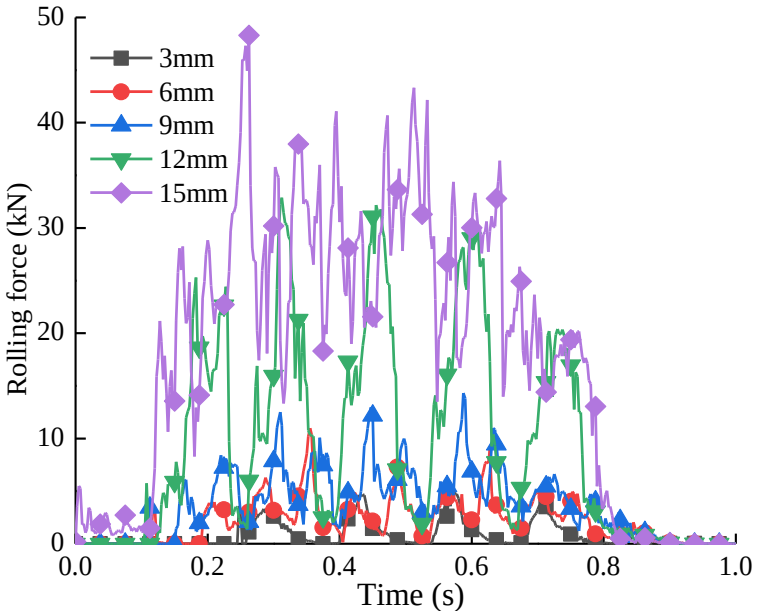

Fig. 12. Rolling force under different penetrations

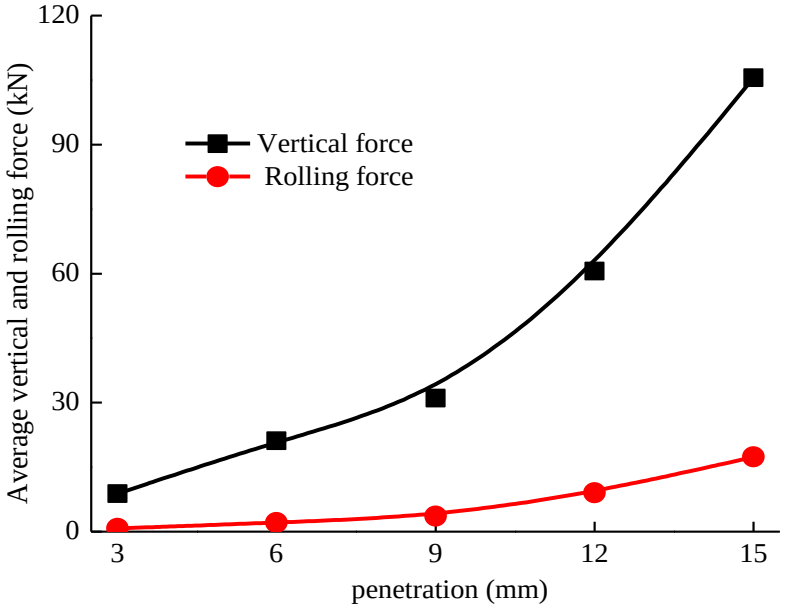

Fig. 13. Average vertical force and rolling force under different penetrations

3.4. INFLUENCE OF PENETRATION ON ROCK CUTTING EFFICIENCY

The specific energy consumption is used to evaluate the rock cutting efficiency of the spherical-tooth hob, which is calculated by the ratio of rock breaking energy to rock breaking volume (Qiao, et al., 2018). A high rock cutting efficiency is accompanied by a low specific energy consumption. The relationship between specific energy consumption and penetration is illustrated in Fig. 14. With the growth of the penetration, the specific energy consumption initially decreases and then increases, reaching a valley value of 42.4 MJ/m^3 when the penetration is increased to 12 mm. It reveals that the rock cutting efficiency of the spherical-tooth hob is the highest at this penetration.

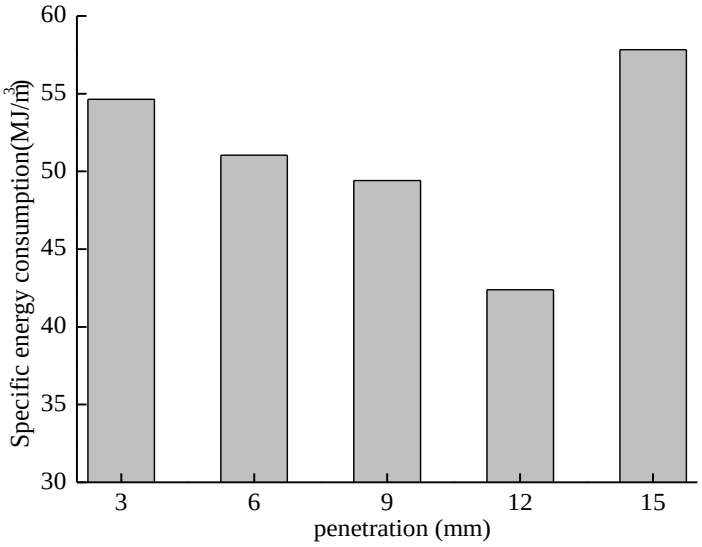

Fig. 14. Specific energy consumption under different penetrations

It can be commented that when the penetration is at a low value (less than 9 mm), only the spherical teeth can contact and cut the rock sample, and there is no synergistic action between the spherical teeth and cutter ring, resulting in a high specific energy consumption. While the penetration is equal to 12 mm, the cutter ring can cut the rock with the aid of the spherical teeth which can damage the rock in advance, leading to a low specific energy consumption and a high rock cutting efficiency. However, When the penetration is greater than 12 mm, the cutter ring will cut rock with a large cutting depth

which could cover up the previous rock cutting effect of spherical teeth. Therefore, excessive rock breaking may occur beneath the cutter ring due to the strong extrusion effect of the cutter ring on rock sample, causing a waste of additional rock breaking energy and an increase of the specific energy consumption. In this sense, for a specific structure of the spherical-tooth hob, it exists an optimal penetration to achieve the highest rock cutting efficiency.

4. ROCK CUTTING EXPERIMENT OF SPHERICAL-TOOTH HOB

The rock cutting experiments by spherical-tooth hob are conducted to further investigate the rock breaking characteristics and compare the simulated results. The rock cutting device is illustrated in Fig. 15. The spherical-tooth hob mentioned in Section 2.1 is installed on the hob carrier through cutter shaft and bolts. The hob carrier can move up and down to achieve a required penetration. To obtain the cutting force of the spherical-tooth hob, multiple group strain gauges are sticked on the hob carrier which can monitor the signal of the cutting forces. The rock sample whose mechanical parameters have been stated in Section 2.2 is put into the steel box. The surrounding of the rock sample is restricted by cement to eliminate the boundary influence of the rock sample. The steel box can move back and forth to realize the rock cutting tests. Three cutting tests with penetration of 3, 9 and 15 mm were carried out in this paper. The cutting velocity of these rock cutting tests is set to 20 mm/s.

The rock breaking states after cutting for the penetration of 9 mm and 15 mm are displayed in Fig. 16. In the case of penetration for 9 mm, some pits are produced on the rock sample due the rolling action of the spherical teeth, as shown in Fig. 16 (a). It can also be found that the rocks between two pits are not severed from the rock sample due to the weak interaction between adjacent spherical teeth. This phenomenon has also been revealed in Fig. 10 (c) obtained from the simulation. Under the circumstance of penetration for 15 mm, as displayed in Fig. 16 (b), it can be seen that a cutting groove is left on the cutting path of the spherical-tooth hob, indicating that the cutter ring has been involved in cutting rock. Meanwhile, some pits can also be found in the groove, but the imprint of these pits seems to be shallow compared with that of these pits produced when the penetration is 9 mm. It is mainly caused by the cutting of the cutter ring. This observed result has also been analyzed in Section 3.1 and 3.2, which is consistent with the

simulation result. According to the above analysis, the rock breaking states obtained from experiment is similar to that obtained from simulation, which could prove the reliability of the simulated results.

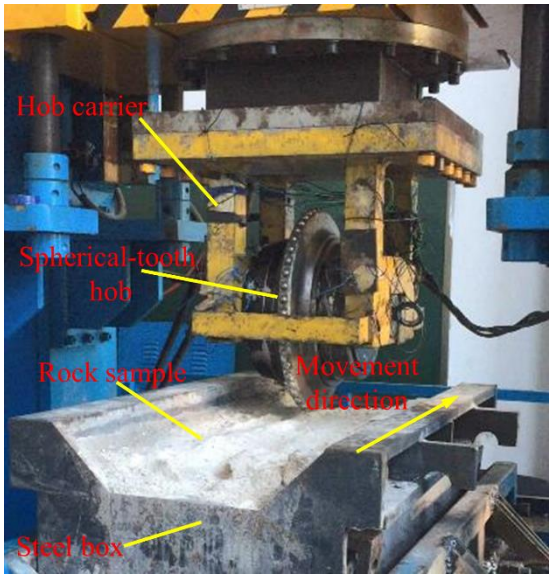

Fig. 15. Rock cutting device

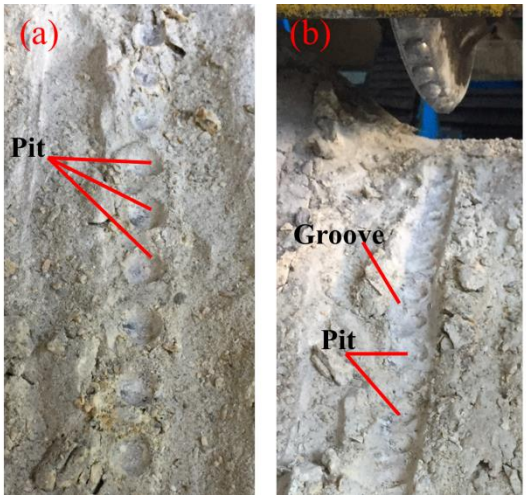

Fig. 16. Rock breaking states beneath the spherical-tooth hob: (a) penetration=9 mm; (b) penetration=15 mm

The comparison of simulated forces and experimental forces is presented in Fig. 17. Overall, both the simulated forces and experimental forces increase with the growth of the penetration. Moreover, the vertical force is much larger than the rolling force regardless of the simulated and experimental results. It still exists some difference between the simulated and experimental forces although the change trends of simulated forces and experimental forces are consistent. The average deviations of vertical and rolling force between simulated and experimental results are about 8% and 12%, respectively. This can be explained by the fact that the interior of rock sample used in experiment is uneven and heterogeneous, which is completely different from the rock sample used in simulation, leading to a certain difference between experimental and simulated forces.

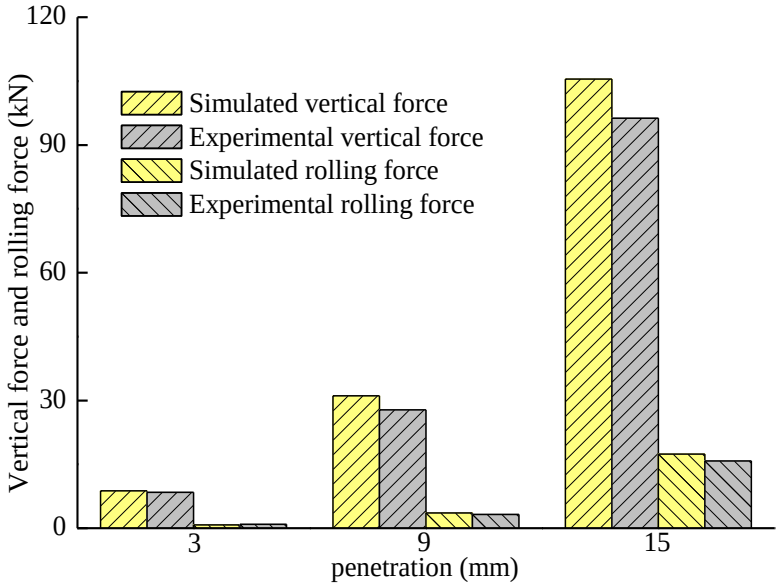

Fig. 17. Comparison of simulated forces and experimental forces

5. DISCUSSION

According to the above analysis, the observed rock breaking states and the change trends of cutting forces from experiment and simulation are consistent. It can be concluded that the penetration has a significant impact on the rock cutting characteristics of the spherical-tooth hob. When the penetration is lower than the height of the spherical tooth

(9 mm), both the simulated and experimental results show that a series of pits caused by the spherical teeth are formed (Fig. 10 (a), (b), (c)and Fig. 16 (a)). While the penetration exceeds the height of the spherical tooth, the cutter ring is involved in the rock cutting process (Fig. 10 (d), (e) and Fig. 16 (b)), a cutting groove is produced by the cutter ring, and the pit imprint caused by the spherical teeth becomes shallower. With the growth of the penetration, the average cutting forces increase rapidly due to the rise of the contact area between the spherical-tooth hob and the rock. When the penetration increases from 3 mm to 15 mm, the vertical and rolling forces increase from 8.84 kN and 0.76 kN to 105.52 kN and 17.37 kN respectively. Especially when the penetration exceeds the height (9mm) of the spherical tooth, the cutter ring will contact and cut the rock sample (Fig. 10), leading to a greater increase speed of average cutting forces. In addition, the vertical force is much larger than the rolling force, and the difference between vertical force and rolling force shows an increasing trend with the growth of the penetration, as described in Section 3.3. It reveals that the rock breaking process induced by the spherical-tooth hob is mainly dominated by the vertical force. These research results above about the rock breaking process and cutting forces caused by the spherical-tooth hob can provide a research basis about the structural design and life prediction of the spherical-tooth hob for the practitioners and the literature in TBM field. On the other hand, the rock cutting efficiency presents a downward trend first and then an upward trend with the growth of the penetration, and the highest rock cutting efficiency is achieved at a penetration of 12 mm (Fig. 14). When the penetration is lower than 12 mm, the rock breaking process completely depends on the extrusion of spherical teeth since the cutter ring does not touch and cut the rock, resulting in a low rock cutting efficiency. While the penetration is larger than 12 mm, the pre-crushing effect made by spherical teeth may be eliminated due to the strong extrusion impact of the cutter ring, leading to a reduction in rock cutting efficiency. Consequently, a proper penetration should be adopted to maximize the rock cutting efficiency of the spherical-tooth hob. It should be noted that the rock between adjacent pits is not broken due to the large spherical tooth spacing and the weak interaction between adjacent spherical teeth, which may reduce the rock cutting efficiency of the spherical teeth. Therefore, a smaller spherical tooth spacing may improve the rock cutting efficiency of spherical-tooth hob. The above analysis can provide a reference to obtain the optimal cutting parameter and the structural parameter of the spherical-tooth hob for the practitioners in TBM engineering.

6. CONCLUSION

In this paper, the rock cutting characteristics of the spherical-tooth hob are investigated based on the rock cutting simulation and experiment. The main conclusions are as follows.

(1) When the penetration is lower than the height of the spherical tooth (9mm), the rock breaking is mainly caused by the spherical teeth, and a series of pits will be produced on the rock sample. While the penetration exceeds the height of the spherical tooth, the spherical teeth could crush rock for the cutter ring in advance, which can relieve the loading condition of the cutter ring. Meanwhile, at such penetration, a cutting groove is produced on the cutting path of the spherical-tooth hob.

(2) The cutting forces including vertical and rolling force fluctuate obviously with the development of the rock cutting, and the cutting forces will not reach zero at its valley value. Meanwhile, the peak values of cutting forces correspond to the moment when a spherical tooth intrudes into the rock sample totally.

(3) The average cutting forces will increase rapidly with the growth of the penetration, and the growth amplitude of the vertical force is much larger than that of the rolling force. When the penetration exceeds 9 mm, the increase speed of cutting forces turns faster due to the action of the cutter ring.

(4) The rock cutting efficiency increase first and then decrease with the growth of the penetration. The optimal penetration corresponding to the highest rock cutting efficiency is 12 mm.

(5) The observed rock breaking states and the change trends of cutting forces from experiment are consistent with that from the simulation, which can confirm the reliability of the similated results.

ACKNOWLEDGMENT

This work is supported by the National Natural Science Foundation of China (No 52005179), the Natural Science Foundation of Hunan Province (No. 2020JJ5365, 2021JJ40355), the Scientific Research Project of Hunan Education Department (No. 20C1153), and the Innovation and Entrepreneurship Training Plan Program for College students in Hunan Province (No. S202210542172).

REFERENCES

Cardu M, Rispoli A, Iabichino G, Oreste P, Vagnon F (2021). Theoretical and Experimental Results from Laboratory Tests by ILCM. Geotechnical and Geological Engineering, 39: 3573-3597

Cho J, Jeon S, Jeong H, Chang S (2013). Evaluation of cutting efficiency during TBM disc cutter excavation within a Korean granitic rock using linear-cutting-machine testing and photogrammetric measurement. Tunnelling and Underground Space Technology, 35: 37-54

Cho J, Jeon S, Yu S, Chang S (2010). Optimum spacing of TBM disc cutters: A numerical simulation using the three-dimensional dynamic fracturing method. Tunnelling and Underground Space Technology, 25(3): 230-244

Deng Y, Yin F, Deng H, Li J, Liu W (2020). Research on crack propagation and rock fragmentation efficiency under spherical tooth dynamic indentation. Arabian Journal of Geosciences, 13(1): 1-9

Entacher M, Schuller E, Galler R (2015). Rock Failure and Crack Propagation Beneath Disc Cutters. Rock Mechanics and Rock Engineering, 48: 1559-1572

Geng Q, Wei Z, Meng H (2016a). An experimental research on the rock cutting process of the gage cutters for rock tunnel boring machine (TBM). Tunnelling and Underground Space Technology, 52: 182-191

Geng Q , Wei Z, Meng H, Chen Q (2016b). Numerical and experimental research on the rock-breaking process of tunnel boring machine normal disc cutters. Journal of Mechanical Science and Technology, 30: 1733-1745

Geng Q, Wei Z, Ren J (2017). New rock material definition strategy for FEM simulation of the rock cutting process by TBM disc cutters. Tunnelling and Underground Space Technology, 65: 179-186

Gertsch R, Gertsch L, Rostami J (2007). Disc cutting tests in Colorado Red Granite: Implications for TBM performance prediction. International Journal of Rock Mechanics and Mining Sciences, 44(2): 238-246

Haeri H, Marji M F (2016). Simulating the crack propagation and cracks coalescence underneath TBM disc cutters. Arabian Journal of Geosciences, 9(2):1-10

Hu X, Du C, Liu S, Tan H, Liu Z (2019). Three-Dimensional Numerical Simulation of Rock Breaking by the Tipped Hob Cutter Based on Explicit Finite Element. IEEE Access, 7: 86054-86063

Jiang B, Zhao G, Gong Q, Zhao X (2021). Three-dimensional coupled numerical modelling of lab-level full-scale TBM disc cutting tests. Tunnelling and Underground Space Technology, 114: 103997

Lin L, Xia Y, Wu D (2020). A hybrid fuzzy multiple criteria decision-making approach for comprehensive performance evaluation of tunnel boring machine disc cutter. Computers & Industrial Engineering, 149: 106793

Lin Q, Cao P, Cao R, Fan X (2019). Acoustic emission characteristics during rock fragmentation processes induced by disc cutter under different water content conditions. Applied Sciences, 9(1): 194

Lin Q, Cao P, Li K, Cao R, Zhou K, Deng H (2018). Experimental study on acoustic emission characteristics of jointed rock mass by double disc cutter. Journal of Central South University, 25(2): 357-367

Liu J, Wan W, Xie S, Wang J (2019a). Indentation characteristics using various indenters: A study based on laboratory and numerical tests. Geotechnical and Geological Engineering, 37(6): 4919-4931

Liu J, Wang J, Wan W, Zhao Y (2018a). The coupled influence of surface and internal crack propagation on rock breakages by indentations in biaxial states. Arabian Journal for Science and Engineering, 43(10): 5067-5077

Liu W, Qian X, Li T, Zhou Y, Zhu X (2019b). Investigation of the tool-rock interaction using Drucker-Prager failure criterion. Journal of Petroleum Science and Engineering, 173: 269-278

Liu W, Zhu X, Li B (2018b). The rock breaking mechanism analysis of rotary percussive cutting by single PDC cutter. Arabian Journal of Geosciences, 11(9): 1-11

Pan Y, Liu Q, Kong X, Liu J, Peng X, Liu Q (2019a). Full-scale linear cutting test in Chongqing Sandstone and the comparison with field TBM excavation performance. Acta Geotechnica, 14(4): 1249-1268

Pan Y, Liu Q, Liu J, Huang X, Liu Q, Peng X (2018). Comparison between experimental and semi-theoretical disc cutter cutting forces: Implications for frame stiffness of the linear cutting machine. Arabian Journal of Geosciences, 11(11): 1-20

Pan Y, Liu Q, Peng X, Liu Q, Liu J, Huang X, Cui X, Cai T (2019b). Full-Scale linear cutting tests to propose some empirical formulas for TBM disc cutter performance prediction. Rock Mechanics and Rock Engineering, 52(11): 4763-4783

Qiao S, Wang A, Xia Y, Liu Z, Liu J, Yang M (2018). Influence of pick layout on the performance of bolter miner cutting head. Mining Science, 25: 161–174.2018.

Tan Q, Zhang K, Zhou Z, Xia Y. (2010), Numerical simulation and experimental observation of rock cracks under action of spherical tooth hob cutter. Chinese Journal of Rock Mechanics and Engineering. 29(1):163-69

Tumac D, Balci C (2015). Investigations into the cutting characteristics of CCS type disc cutters and the comparison between experimental, theoretical and empirical force estimations. Tunnelling and Underground Space Technology, 45: 84-98

Wu F, Yin L, Zhang, H, Gong, Q (2018). Rock fragmentation mechanism and efficiency under inserted-tooth roller cutter by rotary cutting test.China Journal of Highway and Transport, 31: 150-159

Xia Y M, Guo B, Cong G Q, Zhang X H, Zeng G Y (2017). Numerical simulation of rock fragmentation induced by a single TBM disc cutter close to a side free surface. International Journal of Rock Mechanics and Mining Sciences, 91: 40-48

Xia Y, Ouyang T, Zhang X, Luo D (2012). Mechanical model of breaking rock and force characteristic of

disc cutter. Journal of Central South University, 19(7): 1846-1852

Xia Y, Yang M, Lin L, Ji Z, Zhu Z (2021). Effect of blade angles on the shovel muck capacity and wear characteristics for TBM scraper. Arabian Journal for Science and Engineering, 46(5): 5203-5218

Xiao N, Zhou X, Gong Q (2017). The modelling of rock breakage process by TBM rolling cutters using 3D FEM-SPH coupled method. Tunnelling and Underground Space Technology, 61: 90-103

Xue Y, Zhou J, Liu C, Shadabfar M, Zhang J (2021). Rock fragmentation induced by a TBM disc-cutter considering the effects of joints: A numerical simulation by DEM. Computers and Geotechnics, 136: 104230

Zare Naghadehi M, Mikaeil R (2017). Optimization of tunnel boring machine (TBM) disc cutter spacing in jointed hard rock using a distinct element numerical simulation. Periodica Polytechnica Civil Engineering, 1(61): 56-65

Zhai S F, Zhou X P, Bi J, Xiao N (2016). The effects of joints on rock fragmentation by TBM cutters using General Particle Dynamics. Tunnelling and Underground Space Technology, 57: 162-172

Zhang X, Liao Y, Chen Z, Xia Y, Zhang K (2021a). Study on optimum free-face condition of cutting hard rock with tunnel boring machine hob. Periodica Polytechnica Civil Engineering, 65(2): 510-521

Zhang X, Wu J, Hu D, He M, Xia Y (2021b). Comparative study on rock breaking performances by arc and wedge TBM hob with two blades. Geotechnical and Geological Engineering, 39(6): 4581-4591

Zou J, Yang W, Zhang T, Wang X, Gao M (2022). Experimental investigation on hard rock fragmentation of inserted tooth cutter using a newly designed indentation testing apparatus. International journal of mining science and technology. https://doi.org/10.1016/j.ijmst.2022.02.002